International Journal for Multidisciplinary Research (IJFMR)

E-ISSN: 2582-2160 ● Website: www.ijfmr.com ● Email: editor@ijfmr.com

Analysis of the PV/Wind Hybrid Power System Connected to the Grid During Variations of Environmental Conditions And Loads

T. Ashakranthi[1], P. Manjusha[2], S.L. Lavanya[3]

[1]Assisstant Profsessor, Dept.Of Eee, Vsm College Of Engineering, Ramachandrapuram, A.P,India,
[2,3]Associate Professor, Dept.Of Eee, Vsm College Of Engineering, Ramachandrapuram, A.P,India,

Abstract

This paper investigates the modeling, simulation, and dynamic control of a grid-connected photovoltaic (PV)-wind hybrid system serving a large plant with critical variable loads. Maximum power point extraction is applied to the hybrid system to capture maximum power under variable weather conditions. Furthermore, a power flow control strategy is proposed to meet the critical demand of the plant. Modeling and simulation of the proposed hybrid system are performed using MATLAB-Simulink software. Its dynamic performance is analyzed under different environmental conditions. Simulation results have demonstrated the effectiveness of the proposed maximum power point tracking (MPPT) strategies in responding to rapidly varying daytime weather conditions. Furthermore, the results show that when the injected power of the hybrid system exceeds the critical power of the load, the excess power is injected into the utility grid. Otherwise, when the injected power is lower than the critical power demand, the utility grid, in cooperation with the hybrid system, will supply the critical power to the load. Likewise, when the injected power of the hybrid system is not available, the load demand is fully met by the electrical grid.

Keywords: PV, wind, hybrid system, MPPT control, DFIG, load.

Nomenclature

$P_{station-A}$	Maximum power output from station (A)	$\lambda_{ds}, \lambda_{qs}$	Stator flux components in d-q axis
$P_{wind-farm}$	Maximum power from wind farm	V_{ds}, V_{qs}	Stator voltages components in d-q axis
$P_{station-B}$	Maximum power from station (B)	ω_e	Rotational speed of stator flux
P_{plant}	Power demanded by plant	i_{ds}, i_{qs}	Stator currents component in d-q axis
P_{Grid}	Injected power to/from electric grid	i_{dr}, i_{qr}	Rotor current components in d-q axis
I, V	Output current and voltage of PV array	L_m, L_s, L_r	Magnetising, stator inductance, rotor self-inductance
I_{ph}, I_s	Light generated current and saturation current of PV	σ	Leakage factor

N_p, N_s	Number of parallel and series modules	R, L	Resistance, inductance of RL choke
R_s, R_{sh}	Series resistance and parallel resistance	P_{m_pu}	Mechanical power per unit
I_{sc}	Short circuit current at STC (Standard Test Condition)	q	Electron's charge
Ki	Short circuit temperature coefficient	A, K	Constant of Boltzmann and temperature of cell
E_g	Band gab energy of semiconductor used in cell	T, G	Temperature of cell and solar irradiance
I_{rs}	Reversed saturation current at T_{ref}	P, i_{dr}	Number of poles and Rotor converter DC-link current
R_f, L_f	Resistance and inductance of filter	T_{ref}	Referece temperature (25°C)
P_{mech}	Mechanical power of wind turbine	V_w, ω_{ref}	Wind velocity and optimum rotational speed per unit
V_{dc}, C	DC link voltage and DC link capacitor	i_{ms}, m	Stator magnetizing current and Stator modulation factor
λ, β	Tip speed ratio and blade pitch angle	ρ, A_t	Air density and Area swept out by turbine blades
$V_{abc\text{-}conv}, I_{abc\text{-}conv}$	Voltage and current at DC/AC converter	V_{abc}, ω	Voltage at RL filter (grid voltage) and Grid frequency

1.Introduction

The permanent increase in power demand is considered as Doubly fed induction generator (DFIG) is the most commonly used in wind power conversion systems [8-10]. Several surveys have been carried out on wind-PV hybrid power systems [11, 12]. Among them, Rajesh [11] presented a wind-PV hybrid power system to supply continuous power to rural areas. Kumar [12] proposed the connection of wind-PV hybrid power system with power grid. Recently, more challenges occur in grid-connected PV/wind hybrid power system. Among these challenges, improving the quality of injected power, extracting maximum power, and issues related to connecting the hybrid power system to the power grid under any condition [13-15]. This study investigates the detailed dynamic modeling, design, and control of photovoltaic and wind power as a hybrid system interconnected to the power grid and supplying large plants with critical variable loads. The proposed hybrid system consists of two photovoltaic (PV) stations located at different locations and a wind farm integrated into the AC main busbar to improve system efficiency. The maximum power point extraction technique is applied to both the PV stations and the wind farm to capture maximum power under variable weather conditions. The objective of this work is to analyze the performance of the hybrid system under various environmental conditions, such as variations in solar irradiance and wind speed. Furthermore, a power flow control method is proposed to meet the critical load demand of a large-scale plant. The validation and effectiveness of the proposed power flow are evaluated under critical load demand variation, one of the most critical problems today. Furthermore, given that conventional energy sources are limited and have adverse effects on the planet, there has been an urgent need to search for renewable energy sources that do not pollute the Earth. Among these sustainable energy sources, wind and photovoltaic energy can be considered the most promising technologies for electricity production. Wind energy can be used by large generators to generate significant energy capacity. Furthermore, solar irradiation can be utilized as photovoltaic energy. Both photovoltaic and wind power have their own demerits as they are intermittent in nature and highly dependent on weather conditions, besides that photovoltaic power can only be utilized during daytime. Therefore, integrating these renewable energy resources as a hybrid system can be utilized to overcome intermittency and provide high reliability to maintain continuous power output to the power grid or rural areas. In recent years, several investments and researches have been made in PV/wind hybrid power systems, such as Benadli [1-3] who introduced sliding mode control for stand-alone PV/wind hybrid systems. Oskouei [4] proposed a quinary asymmetric inverter used in PV/wind hybrid power systems with battery backup. Laabidi [5] presented a modeling and control strategy for grid-connected PV/wind hybrid power systems. Since the power extracted from the hybrid system is highly dependent on variations in environmental conditions such as solar irradiation and wind speed, maximum power point tracking (MPPT) strategies are therefore essential to capture maximum power under varying weather conditions. Several publications address MPPT control algorithms [1, 3, 6, 7], such as Abbassi [6], who investigated fuzzy logic control to extract maximum power from a hybrid power system.

2. The proposed model of the hybrid energy system

Figure 1 shows the proposed hybrid power system. This system consists of two photovoltaic (PV) plants located at different locations and a wind farm, integrated into the main AC busbar (25 kV busbar). The wind farm

is equipped with a doubly fed induction generator (DFIG). In addition, the wind farm includes a rotor-side converter (RSC) to extract maximum wind power and a grid-side converter (GSC) to adjust the DC busbar voltage to a specified value. The photovoltaic stations (A, B) are exposed to different solar radiation and are installed in different locations. The photovoltaic station is integrated into the Point of Common Coupling (PCC) bus using DC-DC and DC-AC converters. Incremental conductance MPPT. A technique is used to extract maximum output power from the photovoltaic array.A hybrid photovoltaic/wind system supplies a large plant with critical variable loads and the electrical grid. The plant consists of six production lines. Each line contains an induction machine with a nominal power of 2 MVA. When the hybrid system injects more power than the plant's load demand, the surplus is supplied to the electrical grid. Otherwise, if the injected power of the hybrid system is lower than the plant's load demand, the electrical grid supplies the load demand in cooperation with the hybrid system. Furthermore, when the injected power of the hybrid system is unavailable, the plant is supplied entirely by the electrical grid.

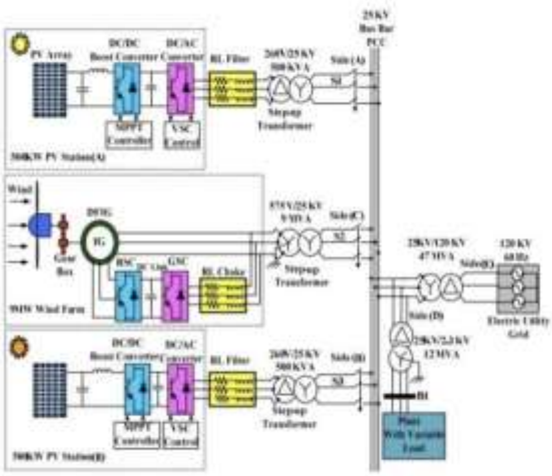

Fig. 1. Hybrid power system model

3.Proposed Hybrid System PowerFlow

Case 1: Hybrid system's injected power exceeds that of the plant

In this case, the injected power of the photovoltaic plants and the wind farm is greater than the plant's demand. Therefore, the hybrid system injects energy into the plant and the electrical grid as follows:

Pstation-A+ Estation-B+Pvind farm = Grid + Pplant

Case 2: Hybrid system input power is lower than the plant's load

BIn this case, the input power of the photovoltaic plants and the wind farm is lower than the plant's demand. Therefore, the power grid will supply the plant's demand in collaboration with the hybrid system. The hybrid system and the power grid will inject power into the plant as follows:

Pstation−A+Pstation−B+Pwindfarm+PGrid=Pplant (2)

Case 3 - Hybrid System Injected Power Unavailable

When the hybrid system's injected power is unavailable, the plant's load demand is fully supplied with electricity, as follows:

PGrid = Pplanta. (3)

The hybrid system's power flow is summarized in the figure.

(a)Pstation-A+Pstation-B+PWindfarm>Pplant

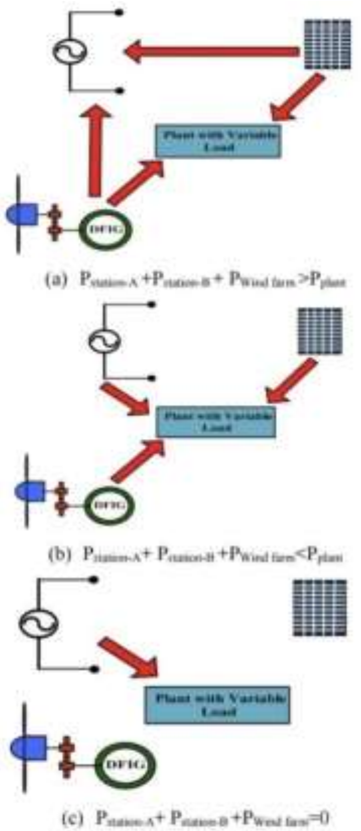

Fig. 2. Graphical representation of power flow

4 Photovoltaic Conversion System

This section presents the electrical modeling of the photovoltaic system and the characteristics of the photovoltaic field. It also discusses the MPPT technique and the DC-AC inverter controller.

4.1 *PV System Model*

Shockley diode-based photovoltaic system modeling has been introduced, as shown in Fig. 3 [8, 16]. The electrical characteristics of a photovoltaic system can be simulated based on variations in environmental conditions, such as solar radiation intensity. The corresponding equation for the current-voltage characteristics of the photovoltaic system can be written as follows [1]:

$$I = N_p I_{ph} - N_p I_s \left\{ \exp\left[\frac{q\left(\frac{V}{N_s} + \frac{R_s I}{N_p}\right)}{KTA} \right] - 1 \right\} - \left(\frac{\frac{N_p V}{N_s} + R_s I}{R_{sh}} \right) \quad (4)$$

$$I_{ph} = \frac{G}{1000}\left[I_{sc} + K_i\left(T - T_{ref}\right) \right] \quad (5)$$

$$I_s = I_{rs}\left(\frac{T}{T_{ref}}\right)^3 \exp\left[\frac{q E_g}{K A}\left(\frac{1}{T_{ref}} - \frac{1}{T}\right) \right] \quad (6)$$

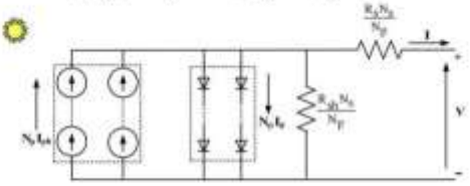

Fig. 3. PV array model.

Detailed specifications of each photovoltaic station are given in Appendix A. Figure 4 shows the current/voltage characteristics and power/voltage characteristics of each photovoltaic array under different solar irradiation intensity conditions.

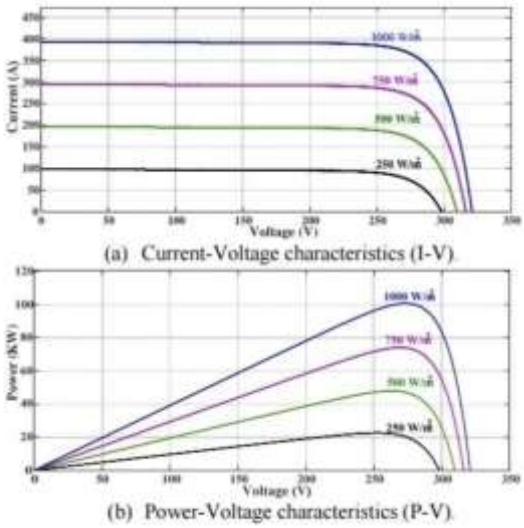

(a) Current-Voltage characteristics (I-V)

(b) Power-Voltage characteristics (P-V)

Fig. 4. Characteristics of PV array.

4.2 *Maximum Power Point Tracking Algorithm*

Maximum power point tracking strategies are used in photovoltaic conversion systems. Since the intensity of solar radiation varies with time, the MPPT technique is used to extract the maximum output power from the photovoltaic array. Previous studies have introduced various MPPTs [1, 6, 7, 17]. In this paper, the incremental conductance MPPT algorithm is used due to its good performance under rapidly changing solar radiation [15, 18, 19]. Figure 5 shows the flowchart for the incremental conductance MPPT technique. The implementation of the MPPT technique in the Simulink model is shown in Figure 6. The incremental conductance strategy depends on the slope of the power-voltage (P-V) curve being equal to zero at the maximum power point (MPP). Furthermore, the derivative of power with respect to voltage (dPp/dV) is positive to the left of the MPP and negative to the right. The mathematical model for this technique is as follows:

Photovoltaic array output power

$$P_{pv} = V_{pv} * I_{pv} \quad (7)$$

$$\frac{dP_{pv}}{dV_{pv}} = \frac{d}{dV_{pv}}[V_{pv} * I_{pv}] = I_{pv} + V_{pv}\frac{dI_{pv}}{dV_{pv}} \quad (8)$$

Then,

$$\frac{dP_{pv}}{dV_{pv}} = 0 \,,\; \frac{dI_{pv}}{dV_{pv}} = -\frac{I_{pv}}{V_{pv}} \quad \text{at the MPP } \Delta V_n = 0 \quad (9)$$

$$\frac{dI_{pv}}{dV_{pv}} > -\frac{I_{pv}}{V_{pv}} \quad \text{Left of the MPP , increment } V_{PV} \quad (10)$$

$$\frac{dI_{pv}}{dV_{pv}} < -\frac{I_{pv}}{V_{pv}} \quad \text{Right of the MPP , decrement } V_{PV} \quad (11)$$

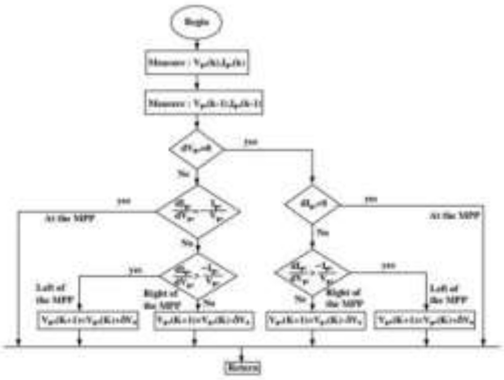

Fig. 5. Flow chart of incremental conductance technique

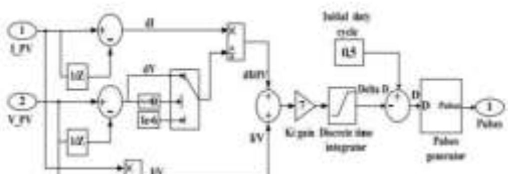

Fig. 6. Simulink model of PV MPPT control

4.3 *DC/AC Converter Controller*

Figure 7 shows the control scheme of the DC/AC converter controller. Its main function is to regulate the DC bus voltage, control the active power injected into the load, and achieve unity power factor at the PCC bus. This control strategy is beneficial due to its decoupled control capability and fast dynamics [14, 15]. Thus,

$$V_{abc} = V_{abc\_conv} - R_f I_{abc\_conv} - L_f \frac{dI_{abc\_conv}}{dt} \quad (12)$$

Transforming Equation (12) into d-q rotating reference frame yield

$$V_{d\_conv} = R_f I_d + L_f \frac{dI_d}{dt} - \omega L_f I_q + V_d \quad (13)$$

$$V_{q\_conv} = R_f I_q + L_f \frac{dI_q}{dt} + \omega L_f I_d + V_q \quad (14)$$

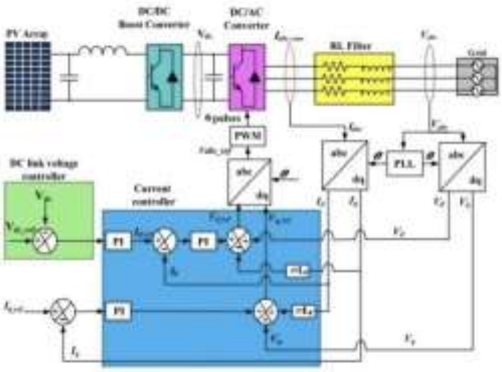

Fig. 7. DC/AC converter control scheme

The phase-locked loop is a closed-loop frequency control strategy. This structure estimates the line voltage angle (0) for the d-q coordinates and synchronizes the converter output voltage with the line voltage and current [20]. Figure 8 shows the control scheme of the phase-locked loop.

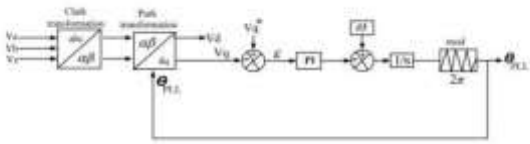

Fig. 8. Block diagram of phase locked loop

4.3.1 *DC Link Voltage Controller*

The DC-link voltage controller regulates the voltage to a specified constant value. The reference voltage is compared with the actual value, and the difference is applied to the PI controller to regulate the voltage to 500 V DC. The output of this controller is used as the forward-axis reference current (Ia rer) for the internal current controller.

4.3.2 *Current Controller*

The current controller loop independently controls the direct axis (Ia) and quadrature axis (I) of the grid currents. The (Ia re) is derived from the disconnection voltage control, while the (I re) is set to zero to maintain unity power factor. By aligning the direct axis of the grid voltage (V) with the grid voltage vector, the quadrature grid voltage (V) is set to zero. Therefore, the injected active power (P) and reactive power (O) can be independently adjusted by I and I respectively [5]. Then,

$$P = \frac{3}{2}\left(V_q I_q + V_d I_d\right) = \frac{3}{2} V_d I_d \quad (15)$$

$$Q = \frac{3}{2}\left(V_q I_d - V_d I_q\right) = -\frac{3}{2} V_d I_q \quad (16)$$

5 Wind Energy Conversion System

This section presents the mechanical modeling of wind turbines and their characteristics. It also discusses RSC and GSC controllers, as well as the MPPT technique..

5.1 *Modeling of Wind Turbine*

A wind turbine is modeled by an aerodynamic input torque driving a doubly fed induction generator. The mechanical power (Pmecs) extracted from the wind turbine is described below [4]:

$$P_{mech} = \frac{1}{2} \rho A_t C_p(\lambda, \beta) V_w^3 \qquad (17)$$

The power coefficient (C_2) represents the turbine's efficiency and depends on the aerodynamics of the blades. The power coefficient (C) can be described as follows:

$$C_p(\lambda, \beta) = 0.5176 \left(\frac{116}{\lambda_i} - 0.4\beta - 5\right) e^{\left(\frac{-21}{\lambda_i}\right)} + 0.0068\lambda \qquad (18)$$

$$\frac{1}{\lambda_i} = \frac{1}{\lambda + 0.08\beta} - \frac{0.035}{\beta^3 + 1} \qquad (19)$$

Detailed specifications of the wind turbine and doubly fed induction generator are presented in Appendix A. Figure 9 illustrates the power characteristic curve of the wind turbine for different wind speeds. It can be seen that the maximum power point is reached at different wind speeds.

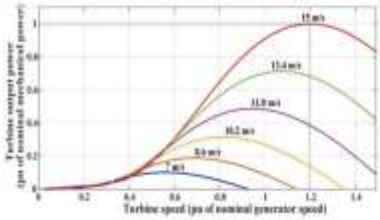

Fig. 9. A Typical wind turbine power characteristics.

5.2 Rotor-Side Converter Controller

The main objective of the RSC is to extract maximum power and control the injected reactive power (Oγ) to maintain the DFIG stator at unity power factor [9, 21]. The stator flux (β) is oriented synchronously along the rotating d axis, βγ = 24, i.e., -0. Therefore, the stator currents and voltages in the rotating d-q reference frame can be described as follows [9, 22]:

$$i_{qs} = -(L_m / L_s) i_{qr} \text{ and } i_{ds} = (1/L_s)\lambda_{ds} - (L_m / L_s) i_{dr} \qquad (20)$$

$$V_{ds} = 0 \text{ and } V_{qs} = \omega_e \lambda_{ds} \qquad (21)$$

The d-q components of the rotor voltage references (V") and (Vr) can be expressed as follows:

$$(V_{dr})^* = (V_{dr})' - (\omega_{slip}) \sigma L_r i_{qr} \qquad (22)$$

$$(V_{qr})^* = (V_{qr})' + (\omega_{slip}) \left(\left(L_m^2 / L_s \right) i_{ms} + \sigma L_r i_{dr} \right) \qquad (23)$$

The stator active power (P), reactive power (O) and electromagnetic torque (Te) can be expressed as follows:

$$P_s = \frac{3}{2}\left[-V_{qs} i_{qs} \right] = \frac{3L_m}{2L_s}(\omega_e \lambda_{ds} i_{qr}) \qquad (24)$$

$$Q_s = \frac{3}{2}\left[V_{qs} i_{ds} \right] = \frac{3\omega_e}{2}(\lambda_{ds} i_{ds}) \qquad (25)$$

$$T_e = \frac{3}{2}\frac{P}{2}\frac{L_m}{L_s}\left[\lambda_{ds} i_{qr} \right] \qquad (26)$$

The RSC control scheme is shown in Fig. 10. The rotor voltage reference on the q-axis (Va) is generated by an MPPT controller. The rotor voltage reference on the d-axis (Va) is created from the reactive power control loop. The reactive power reference (Q*) is set to zero, which ensures that the stator has a power factor equal to unity [10].

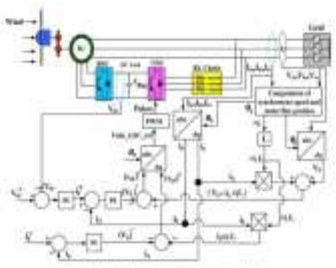

Fig. 11. Grid side converter controller.

5.3 Grid Converter Controller

The main function of the GSC is to maintain the DC link voltage at a constant specified value and a power factor equal to unity at the grid connection point. The grid converter voltage in the d-q synchronous reference system can be expressed as follows [3, 13]:

$$V_d = V_{d1} + Ri_d - \omega_e L i_q + L\frac{di_d}{dt} \quad (27)$$

$$V_q = Ri_q + L\frac{di_q}{dt} + \omega_e L i_d + V_{q1} \quad (28)$$

By aligning the d-axis of the reference system with the grid voltage vector (V), VFV is obtained, therefore V = 0. In this way, the real power (P) and the DC link voltage can be adjusted by (ia), while the reactive power (O) can be controlled by (i), as follows:

$$P_g = \frac{3}{2} V_d i_d \quad (29)$$

$$Q_g = -\frac{3}{2} V_d i_q \quad (30)$$

$$C\frac{dV_{dc}}{dt} = \frac{3m}{4\sqrt{2}} i_d - i_{or} \quad (31)$$

The control structure of the GSC is shown in Fig. 11. The GSC is a current-regulated Pulse Width Modulation (PWM) converter, with current on the forward axis (ia) to adjust the DC bus voltage and current on the quadrature axis (i) to regulate the reactive power exchanged with the grid. The q-axis current reference (in) is set to zero to maintain the grid at a stable power factor. The d-q reference components for the GSC voltage can be described as follows:

$$V_{d1}^* = -(V_d)' + (\omega_e L i_q) + V_d \quad (32)$$

$$V_{q1}^* = -(V_q)' - (\omega_e L i_d) \quad (33)$$

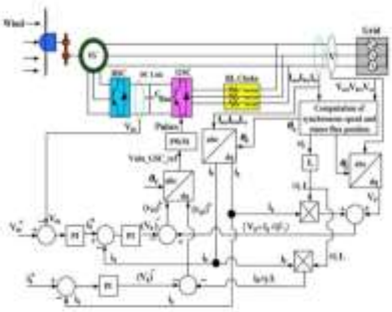

Fig. 11. Grid side converter controller.

5.4 Enhanced MPPT Control Strategy

The maximum power from the wind turbine is extracted at the optimal rotor rotation speed (ω_{ref}). Therefore, as the wind speed varies, the MPPT controller calculates this optimal rotation speed to capture

International Journal for Multidisciplinary Research (IJFMR)
E-ISSN: 2582-2160 • Website: www.ijfmr.com • Email: editor@ijfmr.com

the maximum power from the wind turbine. Common MPPT techniques rely on measuring wind speed and wind turbine characteristics. Therefore, errors in wind turbine modeling and inaccurate sensors will affect the accuracy of the MPPT controller [23]. In this article, an enhanced MPPT control technique based on measuring mechanical power (Pmp) is proposed to determine the optimal rotation speed (w). The MPPT controller flowchart is shown in Fig. 12. The MPPT control strategy is explained as follows:

- First, the controller sets initial values for the mechanical power (Pm-p) and the optimal rotation speed (ω_{ref}).
  the actual mechanical power to calculate the optimal rotation speed (ω_{ref}).
- The controller then calculates the actual mechanical power to calculate the optimal rotation speed (ω_{ref})
- If the mechanical power (PM-PU) is greater than 0.75 p.u., the optimum rotational speed is normally 1.2 p.u. The one corresponding to the maximum power of the wind farm (9 MW).
- If the mechanical power (Pm-pu) is lower than 0.75 p.u., the optimum rotational speed is calculated according to Eq. (29).

The enhanced MPPT control strategy allows the optimal rotation speed to be accurately calculated to track maximum power without the need to measure wind speed. The optimal rotation speed can be expressed as follows [23-25]:

$$\omega_{ref} = \begin{cases} 1.2 & 1 \geq P_{m\_pu} \geq 0.75 \\ -0.67(P_{m-pu})^2 + 1.42(P_{m-pu}) + 0.51 & P_{m\_pu} < 0.75 \end{cases} \quad (34)$$

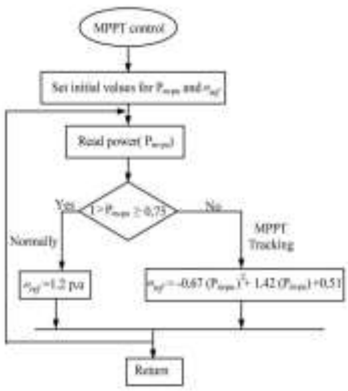

Fig. 12. Flow chart of the MPPT controller.

6 Simulation Results and Analysis

The detailed specifications of the PV-wind hybrid system (Fig. 1) are presented in Appendix A. This section is divided into two parts: 1) Performance of the hybrid power system under different environmental circumstances, such as variations in solar irradiance and wind speed; 2) Validation of the proposed power flow under varying critical plant load demand. The simulation results indicate that the proposed control strategies achieved the desired system performance. Furthermore, the proposed power flow strategy (7/13) satisfactorily meets the critical plant load demand.

6.1 *Performance of the Hybrid Photovoltaic-Wind System*

6.1.1 *Performance of the Photovoltaic Power Plant (A)*

The performance of the photovoltaic power plant (A) is analyzed under changes in solar irradiance, as illustrated in Fig. 13. The surface temperature of the photovoltaic array is kept constant at 25°C throughout the simulation. Fig. 13(a) shows the variation in solar irradiance [26]. This variation shows, for example, the change in irradiance during a day and the shadowing of clouds. Fig. 13(b) shows that the active power injected from the photovoltaic power plant (A) varies with solar irradiance and that the reactive power is zero, so the power factor is unity. Fig. 13(c) shows the three-phase injected current. It can be seen that the DC/AC converter controller regulates the current amplitude based on the injected power. Fig. 13(d) illustrates the efficiency of the system controller. Therefore, the grid voltage is in phase with the injected current due to the unity power factor.

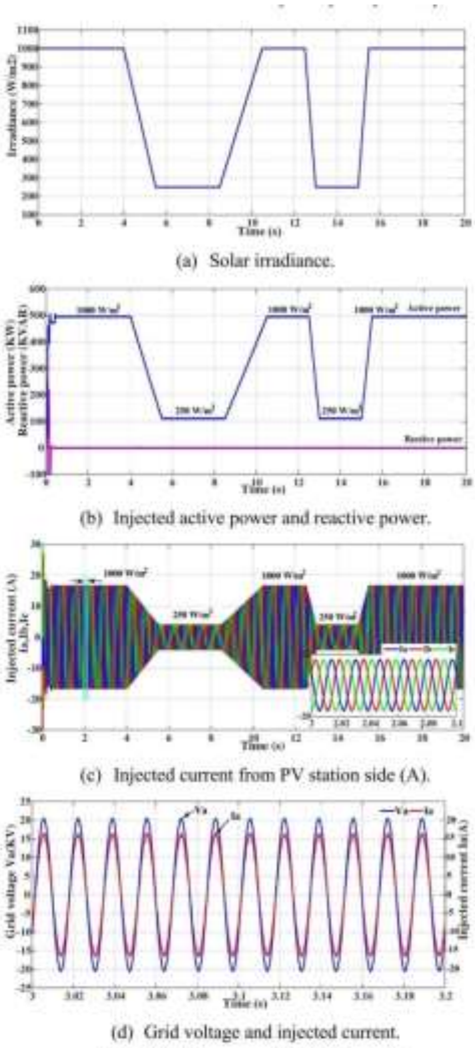

(a) Solar irradiance.
(b) Injected active power and reactive power.
(c) Injected current from PV station side (A).
(d) Grid voltage and injected current.
Fig. 13. Performance of PV station (A).

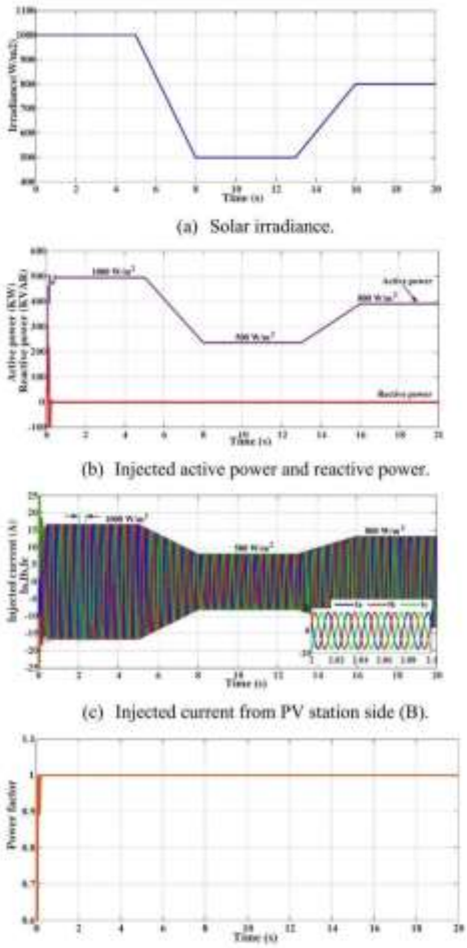

(a) Solar irradiance.
(b) Injected active power and reactive power.
(c) Injected current from PV station side (B).
(d) Power factor of DC/AC converter.
Fig. 14. Performance of PV station (B).

6.1.2 *Photovoltaic Plant (B) Performance*

The performance of the photovoltaic plant (B) is investigated under the influence of solar radiation, as shown in Fig. 14. The change in solar radiation is shown in Fig. 14(a) [27]. This change represents, for example, the shadow of a cloud. Fig. 14(b) shows that the active power injected from the photovoltaic plant (B) is very close to the generated value, so losses are small, and the injected reactive power is zero, implying a unity power factor. Fig. 14(c) shows the injected three-phase current. The change in current amplitude reflects the variation in power from the grid.

The voltage remains constant. Figure 14(d) illustrates that the power factor of the DC/AC converter is very close to one.

International Journal for Multidisciplinary Research (IJFMR)

E-ISSN: 2582-2160 ● Website: www.ijfmr.com ● Email: editor@ijfmr.com

6.1.3 *Wind Farm Performance*

Figure 15 shows the performance of the DFIG wind farm under wind speed variations. The speed variation for gradient winds is represented in Fig. 15(a) [28]. The wind speed ramp is between 15 m/s and 10 m/s. Fig. 15(b) shows that the wind farm's injected active power changes according to wind speed, while the supplied reactive power remains zero, i.e., with a unity power factor. Therefore, the MPPT controller accurately tracks the optimal rotation speed when the wind speed varies continuously. Fig. 15(c) shows the three Phase-directed current injected from the wind farm. It is observed that the RSC controller regulates the current amplitude as a function of the injected power. Fig. 15(d) shows that the GSC controller maintains the DC link voltage fixed at 1150 V, regardless of the magnitude of the injected power.

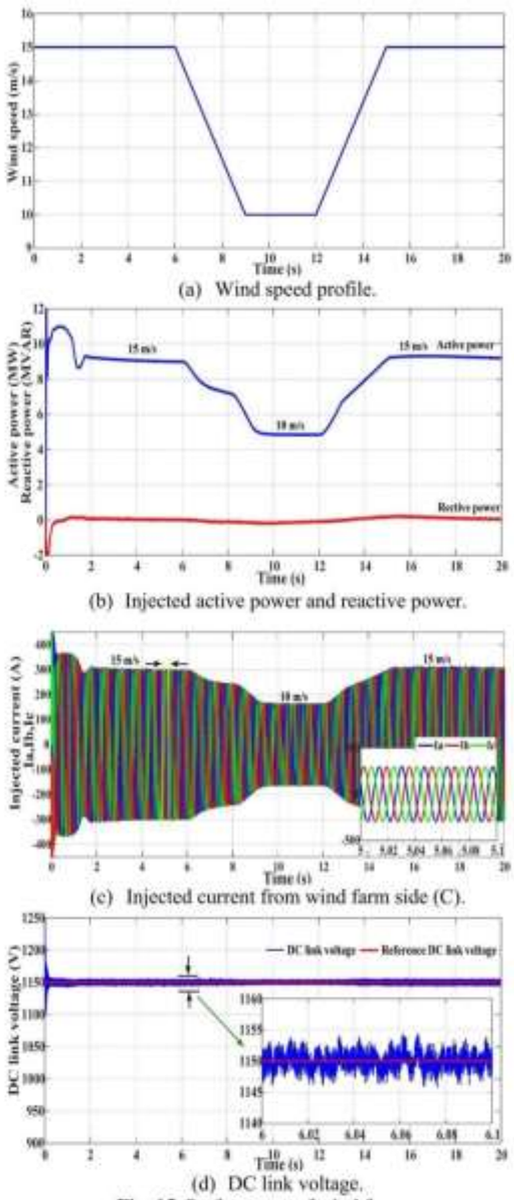

Fig. 15. Performance of wind farm

Figure 16(a) shows the power balance of the hybrid system. It is observed that the power injected from the hybrid system to the grid (PCC-bus) is equal to the sum of the powers injected from the photovoltaic plant (A), the photovoltaic plant (B) and the wind farm. Figure 16(b) shows a constant voltage of the PCC-bus with a peak value of 20 kV per phase (25 kV L-L). The PCC-bus voltage remains constant regardless of the variations in the power injected from the hybrid system.

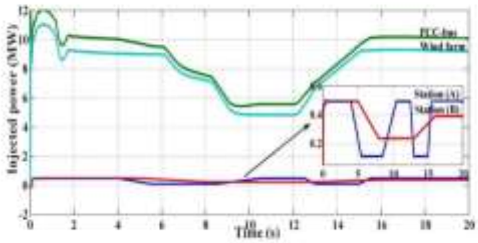

(a) Power delivered to grid side (PCC-bus).

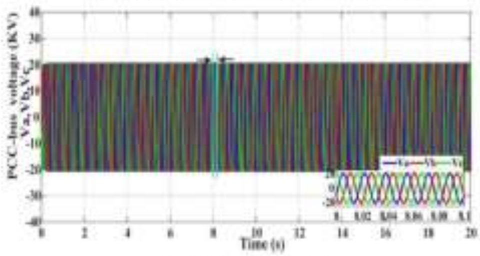

(b) Voltage of PCC-bus.

6.2 ***Validation of the Proposed Power Flow***

6.2.1 ***Hybrid System Injected Power Greater than the Plant Load***

In this case, the power generated by the photovoltaic plants and the wind farm is greater than the power demanded by the plant's critical load. Therefore, the hybrid system will feed the plant's critical load, and the excess power will be injected into the power grid, as shown in Fig. 17(a). Therefore, according to Eq. (1), the hybrid system injects power to the plant and the utility. Fig. 17(b) shows the three-phase load current waveforms. The power demanded by the critical load is 8 MW with 262.3 A from 0 s to 4 s. During the period from 4 s to 8 s, the critical load power decreases from 8 MW to 6 MW with 202.8 A. Subsequently, the critical power of the plant is reduced to 4 MW with 139.3 A from 8 s to 13.5 s. Finally, the critical load power suddenly returns to 6 MW. Figure 17(c) shows a constant load voltage regardless of the variation of the critical load power.

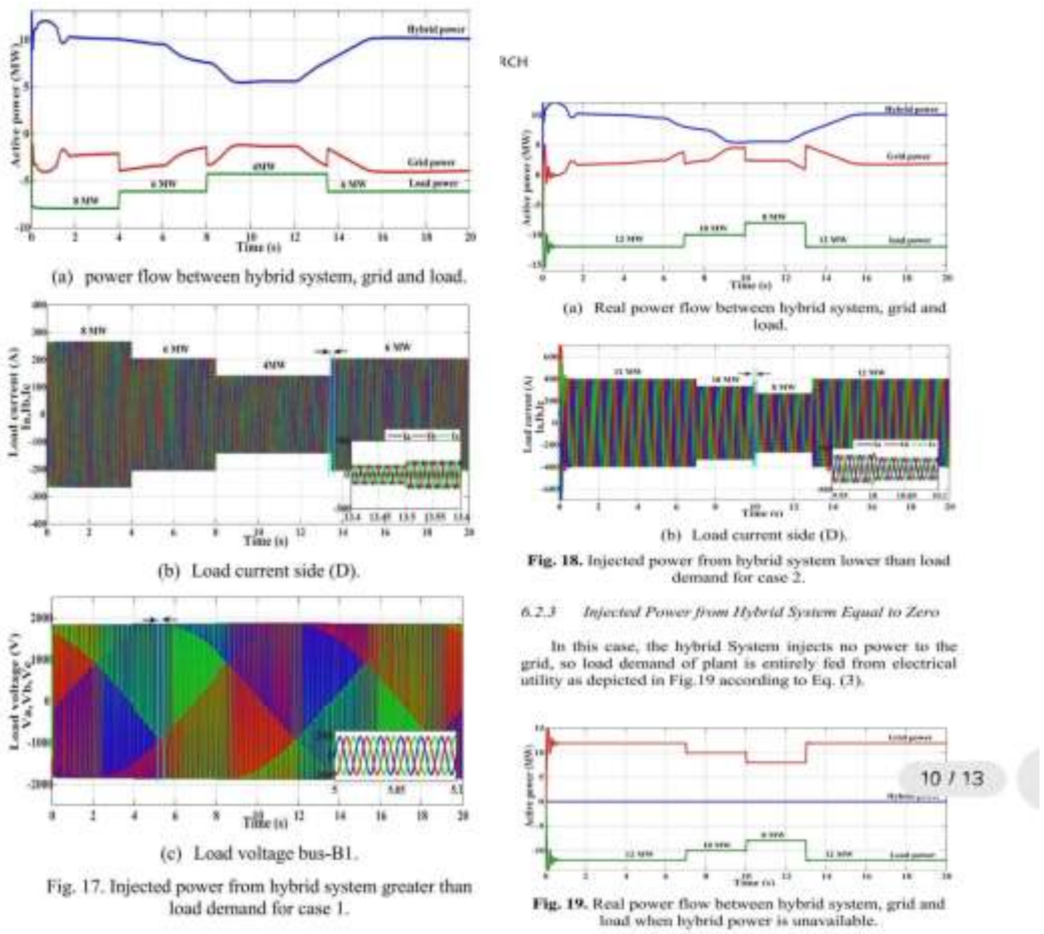

6.2.2 *Hybrid system injected power is lower than load demand*

In this case, the hybrid system's injected power is lower than the plant's critical power demand. Therefore, the power grid, in cooperation with the hybrid system, will supply the critical power demanded to the plant, as shown in Fig. 18(a). Therefore, according to Eq. (2), the hybrid system and the power grid will inject power to the plant's load. Fig. 18(b) shows the three-phase load current waveforms. The critical power demand is 12 MW with 392.2 A from 0 s to 7 s. During the period from 7 s to 10 s, the critical power demand decreases from 12 MW to 10 MW with 325.9 A. Subsequently, the critical power demand decreases to 8 MW with 262.3 A from 10 s to 13 s. Finally, the critical power demand suddenly returns to 12 MW

.

7 Conclusion

In this article, the modeling, simulation, and control of a grid-connected hybrid photovoltaic-wind system have been successfully investigated. The proposed hybrid system consists of two photovoltaic (PV) stations located at different locations and a wind farm, integrated into the main AC busbar, feeding a large plant with critical variable loads. The incremental conductance MPPT technique is applied for both systems.

Photovoltaic power plants extract maximum power under variations in solar irradiance. Furthermore, an improved MPPT control strategy based on mechanical power measurement is applied in wind farms to capture maximum power under changes in wind speed. A power flow control strategy is also proposed to meet the plant's critical load demand. The dynamic performance of the proposed hybrid system is tested under different environmental conditions, such as changes in solar irradiance and wind speed. The validation of the proposed power flow under variations in critical load demand is also evaluated. Simulation results have demonstrated the robustness of the MPPT control strategies to sudden variations in weather conditions during the day. Furthermore, the power flow control strategy satisfactorily meets the plant's critical load demand.

References

1. R.BenadliandA.Sellami,"Slidingmodecontrolof a photovoltaic-wind hybrid system," in Electrical Sciences and Technologies in Maghreb (CISTEM), 2014 International Conference on, 2014, pp. 1-8.
2. J. Hossain, N. Sakib, E. Hossain, and R. Bayindir, "Modelling and Simulation of Solar Plant and Storage System: A Step to Microgrid Technology," International Journal of Renewable Energy Research (IJRER), vol. 7, pp. 723-737, 2017.
3. U. Choi, K. Lee, and F. Blaabjerg, "Power electronics for renewable energy systems: Wind turbine and photovoltaic systems," in Renewable EnergyResearchandApplications(ICRERA),2012 International Conference on, 2012, pp. 1-8.
4. A. B. Oskouei, M. R. Banaei, and M. Sabahi, "Hybrid PV/wind system with quinary asymmetric inverter without increasing DC-link number," Ain Shams Engineering Journal, vol. 7, pp. 579-592, 2016.
5. H. Laabidi and A. Mami, "Grid connected Wind- Photovoltaic hybrid system," in Energy (IYCE), 2015 5th International Youth Conference on, 2015, pp.1-8.
6. R. Abbassi, M. Hammami, and S. Chebbi, "Improvementoftheintegrationofagrid-connected wind-photovoltaic hybrid system," in Electrical Engineering and Software Applications (ICEESA), 2013 International Conference on, 2013, pp. 1-5.
7. R. Koad, A. F. Zobaa, and A. El Shahat, "A Novel MPPT Algorithm Based on Particle Swarm Optimisation for Photovoltaic Systems," IEEE Transactions on Sustainable Energy, 2016.
8. M. K. Hossain and M. H. Ali, "Transient stability augmentation of PV/DFIG/SG-based hybrid power system by parallel-resonance bridge fault current limiter,"ElectricPowerSystemsResearch,vol.130, pp.89-102,2016.
9. A. Parida and D. Chatterjee, "Cogeneration topology for wind energy conversion system using doubly-fed induction generator," IET Power Electronics, vol. 9, pp. 1406-1415, 2016.
10. B. Singh, S. K. Aggarwal, and T. C. Kandpal, "Performance of wind energy conversion system using a doubly fed induction generator for maximum power point tracking," in Industry Applications Society Annual Meeting (IAS), 2010 IEEE, 2010, pp. 1-7.
11. K. Rajesh, A. Kulkarni, and T. Ananthapadmanabha, "Modeling and Simulation of Solar PV and DFIG Based Wind Hybrid System," Procedia Technology, vol. 21, pp. 667-675, 2015.
12. M. Kumar, K. Sandhu, and A. Kumar, "Simulation analysis and THD measurements of integrated PV and wind as hybrid system connected to grid," in 2014 IEEE 6th India International Conference on Power Electronics (IICPE), 2014, pp. 1-6.
13. T. R. Ayodele, A.-G. A. Jimoh, J. Munda, and J. Agee, "Dynamic Response of a Wind Farm Consisting of Doubly-Fed Induction Generators to Network Disturbance,"in Simulation and Modeling Methodologies, Technologies and Applications, ed: Springer, 2013, pp. 131-150.
14. B. E. Strand, "Voltage Support in Distributed Generation by Power Electronics," 2008.

15. S. Gautam, D. B. Raut, P. Neupane, D. P. Ghale, andR.Dhakal,"Maximumpowerpointtrackerwith solar prioritizer in photovoltaic application," in Renewable Energy Research and Applications (ICRERA),2016IEEEInternationalConferenceon, 2016, pp. 1051-1054
16. M. A.-E.-H. Mohamed, "Solar IrradianceEstimation of Photovoltaic Module based on Thevenin Equivalent Circuit Model," International Journal of Renewable Energy Research (IJRER), vol. 5, pp. 971-972, 2015.
17. T. Miyagawa, H. Hayashiya, H. Yoshizumi, T. Furukawa, T. Iwakami, and A. Egami,"Examination of maximization of the photovoltaics electric power use by power distribution system control," in Renewable Energy Research and Applications (ICRERA), 2012 International Conference on, 2012, pp. 1-5.
18. D.Sera,L.Mathe,T.Kerekes,S.V.Spataru,andR. Teodorescu, "On the perturb-and-observe and incremental conductance MPPT methods for PV systems," IEEE journal of photovoltaics, vol. 3, pp. 1070-1078, 2013.
19. S. Hesari, "Design and Implementation of Maximum Solar Power Tracking System Using Photovoltaic Panels," INTERNATIONAL JOURNAL OF RENEWABLE ENERGY RESEARCH, vol. 6, pp. 1221-1226, 2016.
20. A. Althobaiti, M. Armstrong, and M. Elgendy, "Current control of three-phase grid-connected PV inverters using adaptive PR controller," in Renewable Energy Congress (IREC), 2016 7th International, 2016, pp. 1-6.
21. E. Aydin, A. Polat, and L. Ergene, "Vector control ofDFIGinwindpowerapplications,"inRenewable EnergyResearchandApplications(ICRERA),2016 IEEE International Conference on, 2016, pp. 478-483.
22. A. Parida and D. Chatterjee, "Model-based loss minimisation scheme for wind solar hybrid generation system using (grid-connected) doubly fed induction generator," IET Electric Power Applications, vol. 10, pp. 548-559, 2016.
23. M. Zhou, G. Bao, and Y. Gong, "Maximum power point tracking strategy for direct driven PMSG," in Power and Energy Engineering Conference (APPEEC), 2011 Asia-Pacific, 2011, p
24. N. W. Miller, W. W. Price, and J. J. Sanchez-Gasca, "Dynamic modeling of GE 1.5 and 3.6 wind turbine-generators," GE-Power systems energy consulting, 2003
25. V. Rajasekaran, "Modeling, simulation and development of supervision control system for hybrid wind diesel system," 2013
26. T. Haripriya, A. M. Parimi, and U. Rao, "Performance evaluation of DC grid connected solar PV system for hybrid control of DC-DC boost converter," in Intelligent Systems and Control (ISCO), 2016 10th International Conference on, 2016, pp. 1-6.
27. A. Cupertino, J. De Resende, H. Pereira, and S. S. Júnior, "A grid-connected photovoltaic system with a maximum power point tracker using passivity- based control applied in a boost converter," in Industry Applications (INDUSCON), 2012 10th IEEE/IAS International Conference on, 2012, pp. 1-8.
28. G. S. Kaloi, J. Wang, and M. H. Baloch, "Active and reactive power control of the doubly fed induction generator based on wind energy conversion system," Energy Reports, vol. 2, pp. 194-200, 2016.